Role of Inhibitor Aliphatic Chain in the Thermodynamics of Inhibitor Binding to *Escherichia coli* Enoyl-ACP Reductase and the Phe203Leu Mutant: A Proposed Mechanism for Drug Resistance[†]

Irina I. Protasevich,[‡] Christie G. Brouillette,*[,‡] Mark E. Snow,[§] Steve Dunham,[||] J. Ronald Rubin,[§] Rocco Gogliotti,[||] and Karen Siegel[⊥]

Center for Biophysical Sciences and Engineering, University of Alabama at Birmingham, 1025 18th Street South, Birmingham, Alabama 35294, Department of Discovery Technologies, Pfizer Global Research and Development, 2800 Plymouth Road, Ann Arbor, Michigan 48105, Department of Biochemistry, Pfizer Global Research and Development, 10777 Science Center Drive, San Diego, California 92121, and Department of Antibacterial Molecular Sciences, Pfizer Global Research and Development, 2800 Plymouth Road, Ann Arbor, Michigan 48105

Received April 15, 2004; Revised Manuscript Received August 19, 2004

ABSTRACT: The antibacterial target enoyl-acyl carrier protein (ACP) reductase is a homotetrameric enzyme that catalyzes the last reductive step of fatty acid biosynthesis. In the present paper, four 2-(2-hydroxyphenoxy)phenol inhibitors, wherein the 4-position substituent varied from H to *n*-propyl, were studied to determine the contribution of the aliphatic chain to the binding to the wild-type (wt) enoyl-ACP reductase from *Escherichia coli* (FabI) and a drug-resistant mutant, (F203L)FabI, in which phenylalanine 203 is mutated to leucine. Thermodynamic parameters of ternary complex formation (enzyme−NAD^+−inhibitor) were determined by isothermal titration calorimetry. The inhibitor affinity to wt FabI and (F203L)FabI increases with increasing aliphatic chain length, although the corresponding affinity for (F203L)FabI is lower, and also, it shows no detectable binding to the 4-H inhibitor. A distinguishing feature of inhibitor binding to either binary enzyme−NAD^+ complex is the apparent negative cooperativity for binding to the tetramer with half-site occupancy. For both enzymes, binding is enthalpy, ΔH, driven. However, binding ΔH becomes less favorable with increasing aliphatic chain length. Increases in affinity are found to be exclusively due to favorable changes in solvation entropy. Incremental changes in thermodynamic parameters within the series of inhibitors binding to wt FabI and (F203L)FabI are approximately the same. However, absolute differences between the two enzymes for binding to a given inhibitor are significant, suggesting different binding modes. This finding, coupled with a binding site conformation that is likely to be more rigid in the mutant, appears to result in the drug resistance of (F203L)FabI.

Enoyl-acyl carrier protein (ACP)[1] reductase I (FabI) is a key physiological regulator of fatty acid biosynthesis in *Escherichia coli* (*1*) and has been identified as an important target for antibacterial drugs (*2*). *E. coli* FabI is the best characterized enzyme among enoyl-ACP reductases (*3*−*5*). It is a homotetramer ($M_r \sim 28\,000$ per subunit), and the crystal structure shows that each subunit is folded into a single structural domain (*6*, 7). The substrate-binding loop (residues 196−205) is unstructured in the crystal structure of the wild-type (wt) FabI binary complex with a cofactor, (FabI−NAD^+) (*8*), but becomes ordered in the ternary complex with inhibitors, forming further van der Waals interactions through Ala196 and interactions with other residues in the binding loop (*7*). wt FabI binds to a variety of (2-hydroxyphenoxy)phenols, including the widely used biocide triclosan (*3*−*5*), and also binds to other classes of inhibitors, such as diazaborines (*7*, 9−11).

Drug resistance is one of the most serious side effects associated with antibacterial therapy. There are three general mechanisms of drug resistance, including efflux of the drug from the cell and transformation of the drug to an inactive metabolite. In many cases, the loss of sensitivity to inhibitors occurs by a third mechanism, where the resistant bacterial strains encode for an enzyme containing specific amino acid mutations that lower the affinity for the inhibitors. Three mutations in the gene encoding *E. coli* FabI have been identified that lead to resistance against triclosan: Gly93Val,

[†] This work was supported, in part, by NASA cooperative agreement NCC8-24b.

* To whom correspondence should be addressed. Phone: 205-975-5469. Fax: 205-934-3352. E-mail: christie@uab.edu.

[‡] University of Alabama at Birmingham.

[§] Department of Discovery Technologies, Pfizer Global Research and Development.

[||] Department of Antibacterial Molecular Sciences, Pfizer Global Research and Development.

[⊥] Department of Biochemistry, Pfizer Global Research and Development.

[1] Abbreviations: ACP, acyl carrier protein; CD, circular dichroism; DMA, dimethyl acetamide; DMSO, dimethyl sulfoxide; DSC, differential scanning calorimetry; FabI, enoyl-ACP reductase from *E. coli*; ITC, isothermal titration calorimetry; MCPBA, *m*-chloroperbenzoic acid; MIC, minimum inhibitory concentration; NAC, *trans*-2-octenoyl-*N*-acetylcysteamine; NAD, nicotinamide adenine dinucleotide; ASA, accessible surface area; SDS−PAGE, sodium dodecyl sulfate−polyacrylamide gel electrophoresis; T_m, midpoint temperature; Tris, tris(hydroxymethyl)aminomethane; wt, wild type.

10.1021/bi0492509 CCC: $27.50
Published on Web 10/02/2004

Met159Thr, and Phe203Leu (*12*). In the case of Gly93Val and Met159Thr, steric interference with inhibitor binding has been speculated to be a possible mechanism for resistance (*3*−5). Phe203 is located on the opposite side of the binding pocket relative to Gly93 and Met159 but is also part of the same flexible substrate-binding loop, which is disordered in apo wt FabI and its binary complex with NAD^+. The Phe203 mutation to Leu leads to a 6-fold increase in the minimum inhibitory concentration (MIC) for triclosan compared to the wild-type protein with a similar effect on the diazaborines (*4*, *5*). The side chain of Phe203 seems to be important for the formation of the inner surface of the binding pocket and participates in hydrophobic interactions with both types of inhibitors. It is thought that these interactions, specifically resulting from edge-on interactions between the aromatic rings of phenylalanine and the inhibitor, could be weakened in the mutant, thus leading to a decreased binding affinity for either inhibitor (*4*, *13*).

In the present studies, it was of interest to determine and compare the energetics associated with inhibitor binding to wt and Phe203Leu (F203L)FabI, to understand the origin of their reduced potency against this drug-resistant mutant. This information could aid in the development of a more effective class of inhibitors. Evaluation of the thermodynamic parameters of binding, ΔH and ΔS, is helpful to the optimization of inhibitor affinity and specificity, because improved affinity can be achieved by changes in either parameter (*14*, *15*). This approach has also assisted in the interpretation of target-based drug resistance and thermodynamic strategies to minimize its effects. In a series of papers, results from a thermodynamic analysis of HIV protease inhibitor binding have led to an understanding of the molecular mechanism for drug resistance in this target (*16*−*19*). High-affinity inhibitors susceptible to resistance had characteristic binding energetics that were achieved through increases in hydrophobicity and preshaping the inhibitor structure to the binding site. In this paper, energetics of 2-(2-hydroxyphenoxy)phenol analogues binding to wt FabI and (F203L)FabI were determined by isothermal titration calorimetry (ITC). Details of the differences in binding thermodynamics in combination with available crystal structures have led to a proposed mechanism for drug resistance.

EXPERIMENTAL PROCEDURES

Protein Preparation. The expression and purification of the wt FabI containing a His-tag [molecular weight (MW) of monomer, 30 027 Da] were described previously (*1*). Construction, expression, and purification of the F203L mutant have been conducted similar to the methods described earlier for the G93V mutant (*3*). The *fabI*^{F203L} allele was amplified from the chromosome of the triclosan-resistant strain and ligated into the pET15b expression vector. DNA sequencing of the expression construct confirmed the presence of the single point mutation. The His-tagged (F203L)FabI (MW of monomer, 29 993 Da) was then expressed and purified to homogeneity by Ni^{2+}-affinity chromatography using similar methods to those described for the wt FabI (*1*). BL21DE3 *E. coli* cells transformed with the wt FabI expression plasmid were grown in LB media to an OD of ∼1.0 in a 2 L fermentation vessel (Vertis) at 37 °C. Isopropyl-β-D-thiogalactopyranoside (IPTG) was added to 1 mM to induce protein expression. After 4 h at 37 °C, the cells were harvested by centrifugation and brought up in 50.0 mM tris(hydroxymethyl)aminomethane (Tris)-HCl at pH 8.0, 0.3 M NaCl, and 1.0% Triton X-100 with 2.0×10^6 units of chicken egg-white lysozyme, (Sigma L-6876). After ∼15 min at room temperature, $MgCl_2$ was added to 5 mM of the final concentration. Benzonase (American International Chemical Inc. 105-9803; 10−20 μL) was added, and the solution was incubated on ice for 10 min. The cellular debris was removed by centrifugation (12000*g* for 30 min), and the supernatant was then loaded on a 10 mL column of Ni−NTA Superflow slurry (Qiagen 30430). The column was washed with 50.0 mM Tris-HCl at pH 8.0 and 20 mM imidazole. The protein was then eluted with 50.0 mM Tris-HCl at pH 8.0 and 200 mM imidazole. The protein was then dialyzed into the storage buffer, and the concentration was determined as described below. The enzymes were stored at a concentration of 25 mg/mL in 50 mM Tris-HCl buffer at pH 7.5 in the presence of 50% glycerol at −80 °C. Purity was not lower than 95% as determined by sodium dodecyl sulfate−polyacrylamide gel electrophoresis (SDS−PAGE) on a 4−20% gradient Tris-HCl Ready Gel (Bio-Rad) in 25 mM Tris-HCl, 250 mM glycine, and 0.1% SDS at pH 8.3, which was run in a Bio-Rad mini-gel apparatus for 50 min at a constant current of 200 V. The protein was stained by Coomassie Brilliant Blue R-250. Protein concentrations were measured using a calculated extinction coefficient at 278 nm of 15 654 M^{-1} cm^{-1} (*20*). The Lowry procedure based on Peterson's modification of the micro-Lowry method (*21*) was used as an independent method for the protein concentration measurement. The difference between concentration values obtained by the two methods was within experimental error limits.

Sources of Inhibitors. PD048890, PD200828, PD202165, and PD205405 (Figure 1) were synthesized as follows.

PD048890 (2-(2-hyroxyphenoxy)phenol) was prepared according to the methods described in ref *22*.

General Method I: 2-(2-Hydroxyphenoxy)-5-methylphenol. A solution of 2-methoxy-4-methylphenol (2.5 mL, 20 mmol) in dimethyl acetamide (DMA, 40 mL) was treated with potassium *t*-butoxide (2.35 g, 21 mmol) and heated to 100 °C for a period of 5 min. The salt was then treated with 2-fluorobenzaldehyde (2.1 mL, 20 mmol), and the reaction was heated for an additional 3 h at 100 °C. The reaction was then poured onto ice, and the oily residue was extracted into ethyl acetate. The organic extracts were dried over $MgSO_4$, filtered, and concentrated to afford 4.3 g. The crude residue (0.5 g, 2 mmol) and *m*-chloroperbenzoic acid (MCPBA) (50−80%, 0.65 g, 3.7 mmol) were heated in $CHCL_3$ (20 mL) at 50 °C for a period of 20 h. The cooled mixture was extracted twice with $NaHCO_3$ (saturated), dried over $MgSO_4$, filtered, and concentrated. The crude residue was redissolved in methanol (20 mL), treated with a drop of concentrated HCl, and heated to reflux for 1 h. The solvent was removed under reduced pressure and used, as is, for the subsequent step (0.2 g). The residue was dissolved in CH_2Cl_2 (10 mL), cooled on an ice bath, and treated with BBr_3 (0.65 g, 0.26 mmol). The mixture was allowed to stir for 45 min and treated with water, and the solvent was removed under reduced pressure. The residue was dissolved in 1 N NaOH, extracted with CH_2Cl_2, and acidified. The resulting solid was collected by filtration, washed with water, and dried under vacuum to afford 0.114 g of the title compound. MS: 215, M^-. CHN calculated: C, 72.21; H, 5.59; N, 0. Observed:

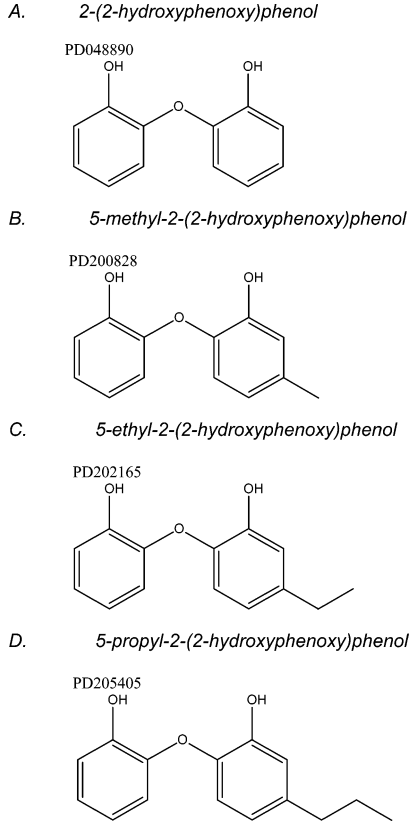

FIGURE 1: Structures of 2-(2-hydroxyphenoxy)phenol inhibitors of FabI.

C, 72.18; H, 5.38; N, 0. NMR [dimethyl sulfoxide (DMSO)-d_6]: δ 9.24 (s, 2H), 6.86 (d, $J = 0.9$ Hz, 2H), 6.71 (d, $J = 1.7$ Hz, 1H), 6.61 (m, 4H), 6.5 (d, $J = 6.7$ Hz, 1H), 2.18 (s, 1H).

5-Ethyl-2-(2-hydroxyphenoxy)phenol was prepared by general method I. MS: 229, M^-. CHN calculated: C, 73.03; H, 6.13; N, 0. Observed: C, 73.35; H, 6.03; N, 0. NMR (DMSO-d_6): δ 9.26 (s, 1H), 9.22 (s, 1H), 6.87 (d, $J = 3.9$ Hz, 2H), 6.74 (d, $J = 1.6$ Hz, 1H), 6.62 (m, 4H), 6.56 (d, $J = 1.4$ Hz, 1H), 2.48 (q, $J = 3.4$ Hz, 2H), 1.12 (t, $J = 6.5$ Hz, 3H).

5-Propyl-2-(2-hydroxyphenoxy)phenol was prepared by general method I. Mp: 87 °C. CHN calculated: C, 73.75; H, 6.60; N, 0. Observed: C, 73.48; H, 6.64; N, 0. NMR ($CDCl_3$): δ 7.05−6.63 (m, 7H), 5.64 (s, 1H), 5.50 (s, 1H), 2.53 (t, $J = 7.3$ Hz, 2H), 1.61 (sext, $J = 7.3$ Hz, 2H), 0.84 (t, $J = 7.3$ Hz, 3H).

Nondenaturing Gel Electrophoresis (Native PAGE). Proteins were electrophoresed at 4 °C on a 4−20% gradient Tris-HCl Ready Gel (Bio-Rad) in 25 mM Tris-HCl and 250 mM glycine at pH 8.3. The high molecular weight calibration kit for native electrophoresis (Amersham Pharmacia) was used as standards. The gel was prerun for 20 min at a constant current of 70 V before the samples were loaded. Proteins were run for 15 min with a constant current of 70 V and then for 19 h at a constant current of 110 V and stained by Coomassie Brilliant Blue R-250.

Spectroscopic Assay of FabI and (F203L)FabI. FabI and (F203L)FabI enzyme activities were assayed spectrophotometrically by monitoring the decrease in absorption at 340 nm using an adaptation of the spectrophotometric assay of Bergler et al. (*23*). Standard reactions contained 200 mM 8:1-NAC, 100 nM of homogeneous FabI (concentration based on the monomer) or (F203L)FabI, 200 mM NADH, and 0.1 M sodium phosphate at pH 7.5, in a final volume of 200 mL. The reactions were performed at room temperature in 96-well microtiter assay plates (Costar). The change in optical density was continuously monitored for 15 min by a SpectraMax Plus plate reader (Molecular Devices), and the reaction rate was calculated from the slope of the linear portion of the trace. Inhibition by the phenoxyphenol inhibitors was determined using a modification of the above assay. As previously observed for triclosan, only inhibitor binding to the E-NAD^+ form of the wt enzyme is detectable. Triclosan binding to the apoenzyme and E-NADH form is not measurable, although binding can be detected to the E-NADH form of the F203L mutant (*13*). To avoid possible contributions from slow inhibitor binding kinetics, similar conditions to those used for triclosan were followed here, which primarily required a preincubation step with the enzyme, NAD^+, and inhibitor prior to initiation of the enzyme reaction (*13*, *24*). Dilutions of the inhibitors in DMSO (1% final concentration of DMSO) were added to the enzyme and NAD^+ (100 nM monomer and 200 μM final concentrations, respectively) and allowed to incubate for 30 min at room temperature prior to the addition of the 8:1 NAC substrate and NADH (both at 200 μM). All solutions were in 100 mM sodium phosphate buffer at pH 7.5. The reactions were performed at room temperature in 96-well microtiter assay plates (Costar). The change in optical density was continuously monitored for 15 min by SpectraMax. As for the reaction in the absence of the inhibitor, the reaction rate in the presence of the inhibitor was calculated from the slope of the linear portion of the trace. Relative inhibition of the enzyme, based on differences in initial velocities with and without the inhibitor, were used to infer a rank ordering of inhibitor efficiency. Technical difficulties related to poor substrate solubility prevented further studies to establish inhibitor K_i and specific mechanism of action, and calorimetry was, instead, pursued to establish binding affinities as well as thermodynamic parameters of binding.

Circular Dichroism (CD). CD spectra were recorded on an Olis DSM 1000 CD spectrophotometer equipped with the thermostated platform and programmable circulating water bath. The cells had a path length of 0.02 and 1.0 cm, respectively, for protein concentrations of 0.05−0.125 mg/mL for far-UV spectra and 0.72−1.62 mg/mL for near-UV spectra. Spectra were recorded from 260 to 190 nm for far-UV and from 320 to 250 nm for near-UV in 1-nm steps with a variable scan speed. The molar ellipticity values were calculated according to the following expression: $[\Theta] = (\Theta/10)(106.5/lc)$, where Θ is the ellipticity in millidegrees, 106.5 is the mean residues molecular weight in grams per mole, l is the path length in centimeters, and c is the concentration of the protein in grams per liter. The value $[\Theta]$ has the units of deg cm^2 $dmol^{-1}$. To obtain the content of the secondary structure, the CD spectra were deconvoluted from 200 to 260 nm by the CD spectroscopy deconvolution software developed by Gerald Böhm (Institut für Biotechnologie Martin-Luther-Universität Halle-Wittenberg, Germany, 1998). The software provides a database of 23 sets of spectra derived from proteins of known secondary structure for standardization. For thermal unfolding, the temperature of the sample was increased at an average rate of 0.7 K/min in temperature

steps of 2 K (an incubation time of 1 min at each temperature). A total of 10 scans from 220 to 230 nm were recorded at each temperature.

Differential Scanning Calorimetry (DSC). Calorimetry was carried out on a differential scanning microcalorimeter (Nano-DSC, CSC) in 0.299 mL cells at heating rates of 1 and 2 K/min. Heating rate did not influence the unfolding parameters. An external pressure of 2.0 atm was maintained during all DSC runs to prevent possible degassing of the solutions upon heating. Protein concentrations were 0.25−0.35 mg/mL in 10 mM Na-phosphate buffer (pH 7.5), 1 mM EDTA, 1% (v/v) glycerol, and 2% (v/v) DMSO. The heat capacity curves were corrected for the instrumental baseline. DSC data were analyzed with the MicroCal Origin software, from which the unfolding temperature (T_m) and the calorimetric (ΔH_{cal}) and van't Hoff (ΔH_{vH}) unfolding enthalpies were obtained. The non-two-state transition model was used to fit experimental unfolding curves in the absence and presence of inhibitors.

ITC. Calorimetric titrations were carried out with a VP-ITC microcalorimeter (MicroCal, Inc., Northampton, MA). The enzyme concentration in the stirred cell (400 rpm) was 8.00 or 13.0 μM (based on the protein monomer), and the syringe contained 250 μM inhibitor. After the initial injection of 2 μL (which was not used in data fitting), 30 injections of 8 μL each were delivered at 210-s intervals. Heats of inhibitor dilution were measured by injecting the inhibitor solution into the buffer solution and were subtracted from the experimental curves prior to data analysis. Experiments were conducted in 10 mM Na-phosphate buffer (pH 7.5), 1 mM EDTA, 1% (v/v) glycerol, and 2% (v/v) DMSO in the presence of 0.5 mM NAD^+ at 15, 20, 25, 27.5, and 30 °C (experimental temperatures were within 0.02 °C of the nominal values). In this temperature range, ΔH is well-approximated as a linear function of T, where $\Delta C_p = (\Delta H_{T_2} - \Delta H_{T_1})/(T_1 - T_2)$ and ΔC_p is the change in heat capacity at constant pressure upon binding. Data were fit to a single binding site model (*25*, 26) using Origin software (version 5.0, MicroCal, Inc.). The binding enthalpy (ΔH), association constant (K_a), stoichiometry (n), and binding entropy (ΔS) were obtained.

Solvent-Accessible Surface Area (ASA) Estimations and ΔC_p Calculations Based on X-ray Structure Analysis. The ASAs of the proteins were determined from the crystal structures of the FabI−NAD^+ binary complex (PDB 1DFI, *10*), and the FabI−NAD^+ diazaborine ternary complex (PDB 1DFH, *10*) by the procedure of Connolly (*27*) with a probe radius of 1.4 Å using the Quanta software (Molecular Simulations Inc., San Diego, CA, 1997). Water, cofactor, and inhibitor molecules in the folded structure were removed, and the cavity surface was included for calculations of ASA. The difference in the buried surface of apolar (ΔASA_{apolar}) and polar (ΔASA_{polar}) side-chain groups because of the ordering of the substrate-binding loop upon complex formation was calculated using the ASAs of wt FabI in the binary complex and wt FabI in the ternary complex with the inhibitor and ASA of the models of the protein with the extended loop conformation (ASA_{model}). The ASA of the loop with an extended conformation in solution was calculated according to Baker and Murphy (*28*) by the ASA values of amino acid residues obtained for tripeptides. The ΔASA_{apolar} and ΔASA_{polar} were obtained for apolar and polar contributions as $ASA_{model} - ASA_{whole}$. $\Delta C_{p(loop)}$ was calculated using the empirical equation $\Delta C_p = 1.836\ \Delta ASA_{apolar} - 1.129 \Delta ASA_{polar}$ (J K^{-1} mol^{-1}) (*28*, *29*).

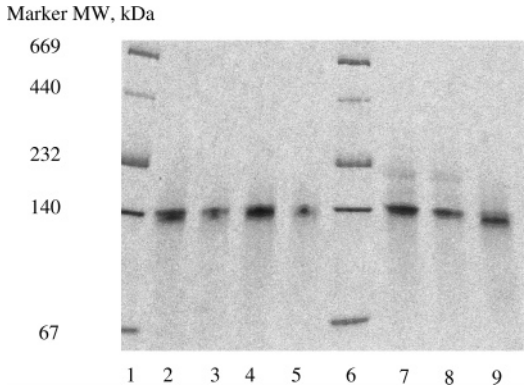

FIGURE 2: Native-PAGE analysis of wt FabI (lanes 2−5) and (F203L)FabI (lanes 7−9). Lane 2, 14 μg of wt FabI; lane 3, 7 μg of wt FabI; lane 4, 14 μg of wt FabI; lane 5, 7 μg of wt FabI in the presence of 1 mM TCEP; lane 6, 14 μg of molecular weight markers; lane 7, 7 μg of (F203L)FabI; and lane 8, 14 μg of (F203L)FabI in the presence of 1 mM TCEP. Lanes 1 and 6 contain molecular weight markers.

RESULTS AND DISCUSSION

Comparative Characterization of wt FabI and (F203L)-FabI. Several structural features were compared to confirm that there are no significant global structural changes in the F203L mutant compared to the wild-type enzyme. As described next, these results indicate that, according to the methods used, the secondary, tertiary, and subunit architecture of wt FabI tetramer are not noticeably changed by the Phe203 to Leu substitution.

Results from native gel electrophoresis show that both wt FabI and (F203L)FabI are tetramers (MW = 120 108) at the concentrations used in ITC and DSC experiments (Figure 2). Far- and near-UV CD indicate that the secondary and tertiary structures of the protein are essentially identical (Figure 3). A small difference in the far-UV spectra is seen, and this may be explained by the likelihood that in apo (F203L)FabI, the flexible substrate-binding loop is ordered, unlike that for the wt (to be discussed further below). Similar secondary structure is observed in the crystal structure of wt FabI, with small differences probably derived from the presence of NAD^+ in the latter (Table 1).

Figure 3B shows the near-UV CD spectra of wt FabI and (F203L)FabI, which are identical in both shape and intensity of the peaks. Near-UV CD spectra reflect the combined contribution of all aromatic amino acid residues: tryptophan, tyrosine, and phenylalanine. wt FabI contains only 1 tryptophan (Trp^{82}), 7 tyrosines, and 10 phenylalanine residues. The invariability of the near-UV CD upon mutation suggests that the local structure and environment of the aromatic residues do not change significantly with the F203L mutation. There is a small positive peak at 296 nm because of Trp, which is not disturbed by mutation. This is not surprising, because Trp^{82} is located very far from the substrate-binding loop. The lack of change by the loss of Phe at 203 is probably due to the lack of structure in the loop containing Phe203 in the apo wt enzyme.

Thermal Unfolding of wt FabI and (F203L)FabI. The temperature-induced unfolding of both wt FabI and

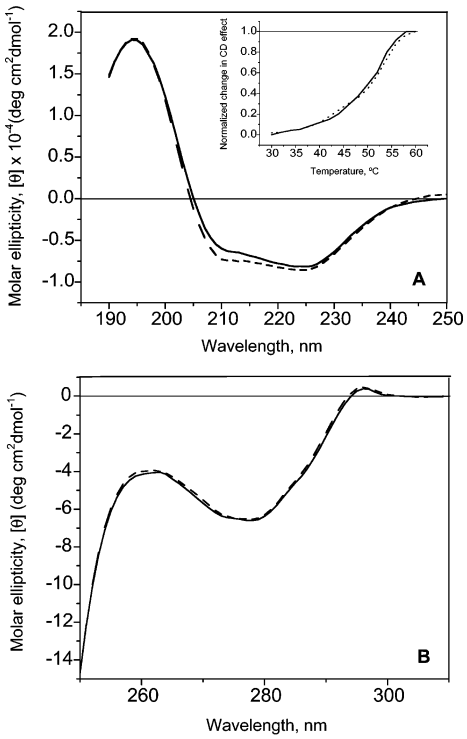

FIGURE 3: CD spectra of apo wt FabI and (F203L)FabI. (A) CD spectra of wt FabI (—) and (F203L)FabI (- - -) in the far-UV region in 10 mM HEPES at pH 7.5 and 22 °C. The protein concentration was 0.45 mg/mL. The inset shows the temperature dependence of the normalized CD signal change at 225 nm for wt FabI (—) and (F203L)FabI (•••). (B) CD spectra of wt FabI (—) and (F203L)-FabI (- - -) in the near-UV region in 10 mM HEPES at pH 7.5 and 22 °C. The protein concentration was 1.62 mg/mL.

Table 1: Secondary Structure of the wt FabI and (F203L)FabI

	wt FabI[a]	(F203L)FabI[a]	FabI−NAD^{+}[b]
α-helix (%)	32.8 ± 0.4	32.4 ± 0.6	37.9
β-sheet (%)	16.9 ± 0.2	17.5 ± 0.3	13.8

[a] Derived from far-UV CD as described in the Experimental Procedures. [b] Derived from the crystal structure of the binary complex FabI−NAD^{+} (as reported in PDB 1DFI, *10*).

(F203L)FabI was monitored by CD at 222 nm and by DSC as a direct method to probe the protein stability and unfolding cooperativity. Parts A and B of Figure 4 show that the unfolding T_m for both wt FabI and (F203L)FabI and the shape of their excess heat capacity profiles are very similar, including the presence of a lower temperature shoulder. Both wt FabI and (F203L)FabI excess heat capacity functions can be represented as two overlapping non-two-state transitions centered at 48.2 ± 0.6 and 52.5 ± 0.2 °C. Far-UV CD thermal unfolding experiments support this analysis. Unfolding profiles of both proteins are very similar (inset curves of Figure 3A) and demonstrate that the secondary structure undergoes two transitions with midpoints at 45 ± 2 and 53.0 ± 0.5 °C, in good agreement with the DSC transition temperatures. The main transition of both proteins is characterized by a ΔH_{cal} equal to 972 ± 12 and 1018 ± 14 kJ/mol for tetramers of wt FabI and (F203L)FabI, respectively, which is ~70% of the total unfolding enthalpy. The ΔH_{vH} is equal to 943 ± 8 and 960 ± 8 kJ/mol for wt FabI and (F203L)FabI, respectively. For both proteins, the $\Delta H_{vH}/\Delta H_{cal}$ ratio, which relates to the number of cooperative units in the molecule (*30*), is very close to unity (0.97 and 0.94

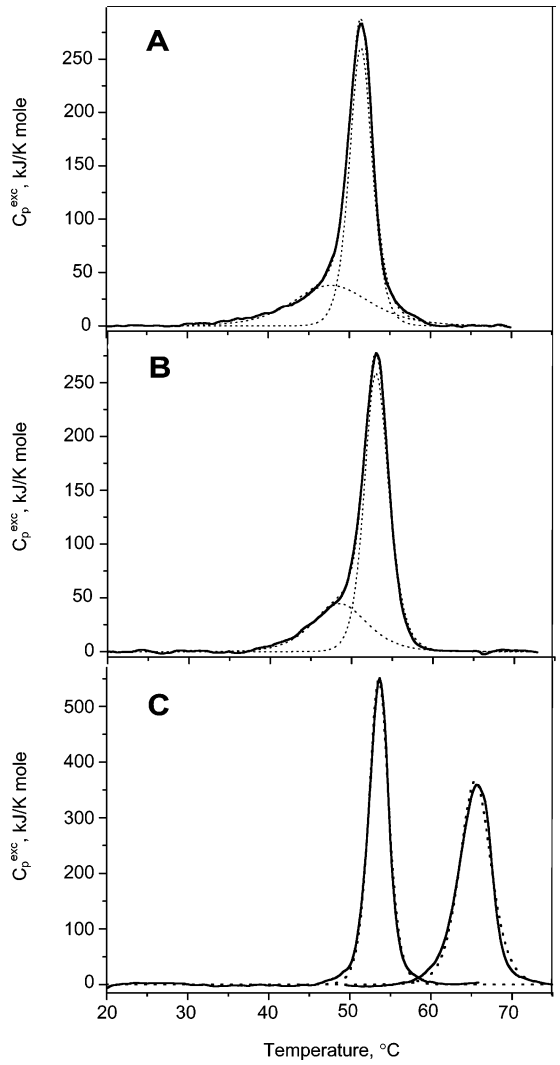

FIGURE 4: DSC of apo wt FabI, (F203L)FabI, and their ternary NAD^{+} inhibitor complexes in 10 mM Na-phosphate buffer at pH 7.5, 2% DMSO, 1 mM EDTA, and 1% glycerol. (A) Temperature dependence of excess heat capacity of apo wt FabI fit to two non-two-state transitions. (B) Temperature dependence of excess heat capacity of apo (F203L)FabI fit to two non-two-state transitions. (C) Excess heat capacity profiles for the ternary complexes of wt FabI−NAD^{+}−PD0205405 (right curve) and (F203L)FabI−NAD^{+}−PD0205405 (left curve), combined into a single panel. Each is fit to a single non-two-state transition.

for wt FabI and (F203)FabI, respectively), indicating that the structural unit, which cooperatively unfolds in the main transition, is the tetramer. The cooperative unit of the smaller, lower temperature transition yields a different result that may shed light on the structural differences between the two apoenzymes. The $\Delta H_{vH}/\Delta H_{cal}$ ratios for wt FabI and (F203L)FabI are 0.6 and 1.0, respectively. For the wt protein, approximately half of the tetramer behaves as a single cooperative domain (the entire tetramer of the mutant is involved in this transition), while the larger, higher temperature transition for both proteins represents a conformational change (i.e., unfolding) for which the entire tetramer participates. The changes in far-UV ellipiticity that accompany the minor transition indicate that about 40% of the secondary structure is lost in both proteins (inset of Figure 3A). The two transitions could, therefore, represent a two-step unfolding process, wherein the cooperativity of the first step is increased in the mutant because of the folding of the

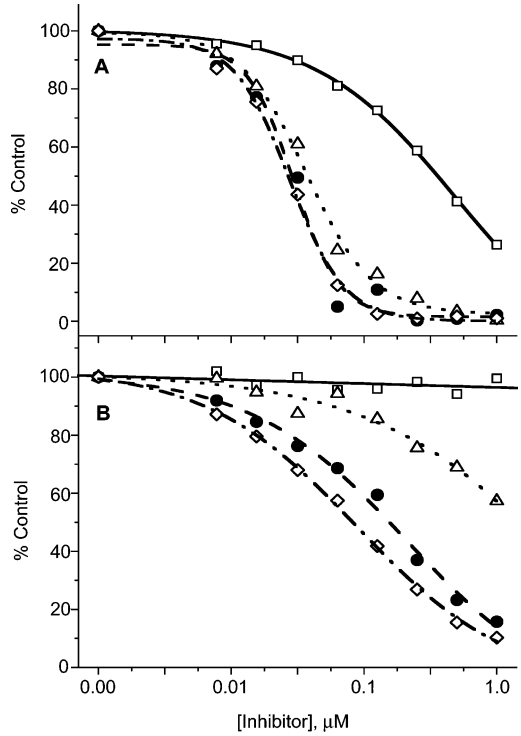

FIGURE 5: Initial velocities of product formation for wt FabI and (F203L)FabI as a function of the inhibitor concentration. All reaction rates were normalized to the rate in the absence of the inhibitor (100% control). (A) wt FabI. (B) (F203L)FabI. 048890 (□), 200828 (△), 205405 (●), and 202165 (◇).

substrate-binding loop containing residue 203. Apparently, the structural architecture that divides the protein into two domains of different stability is not coincident with the subunit architecture that gives rise to the tetramer, because a portion of the tetramer remains intact above the minor transition.

Thermal Unfolding of wt FabI and (F203L)FabI Complexes with PD205405. Figure 4C shows the temperature dependence of the excess heat capacity of wt FabI−NAD^+−PD205405 and (F203L)FabI−NAD^+−PD205405 complexes. The wt FabI complex unfolding curve is shifted higher by 13 °C, whereas the shift in the T_m of the (F203L)FabI complex is only 1 °C. The significant difference in inhibitor affinity between the wt enzyme and the mutant may explain the differences in the T_m shifts. Unlike the unfolding of the apoenzymes, both curves are almost symmetrical and well-fit to a single non-two-state transition, suggesting an improvement in the cooperativity of unfolding. In these ternary complexes with the inhibitor, the cooperative unfolding unit for both proteins is a dimer, rather than a tetramer, as in the case of the main transition for the apoenzymes, because the $\Delta H_{vH}/\Delta H_{cal}$ ratio ranges from 0.4 to 0.6.

Inhibition of wt FabI and (F203L)FabI by 2-(2-Hydroxyphenoxy)phenols. The ability of PD048890 and aliphatic side-chain analogues to inhibit wt FabI and (F203L)FabI was addressed in an *in vitro* spectrophotometric assay using the enoyl-ACP substrate analogue, *trans*-2-octenoyl-*N*-acetylcysteamine (8:1-NAC). Relative inhibition of wt FabI (Figure 5A) and (F203L)FabI (Figure 5B) by each inhibitor is shown in a plot of normalized initial velocities of product formation as a function of the inhibitor concentration. No attempt was made to determine the mechanism of inhibition, although it is known that for the diazaborines and triclosan inhibitors, binding is exclusively to the E-NAD^+ form of the enzyme, and for triclosan, it is competitive with NADH (diazaborines are irreversible inhibitors) (*7*, *24*). Like triclosan, the 2-(2-hydroxyphenoxy)phenols studied here showed no inhibition of wt FabI in the absence of NAD^+. X-ray crystal structures of PD048890 bound to FabI also show that the inhibitor binds in a similar position in the active-site pocket as triclosan and diazaborines (unpublished data). It can be seen that inhibition is progressively greater with increasing aliphatic chain length for both enzymes, whereas inhibition of (F203L)FabI is uniformly weaker across the series of inhibitors. Binding affinities and a mechanism for the resistance of (F203L)FabI to inhibition by these inhibitors was sought through calorimetric measurements described next.

Energetics of wt FabI and (F203L)FabI Binding to the Cofactor. Previously, thermodynamic parameters for NADH binding were obtained by ITC experiments for *E. coli* FabI (*24*) and *M. tuberculosis* enoyl reductase (InhA) (*31*). The K_d values were 5.4 ± 0.9 μM for wt FabI and 2 ± 0.8 μM for InhA, with stoichiometries of 0.91 ± 0.01 per wt FabI monomer and 1.0 ± 0.1 per InhA monomer. In the present paper, K_d values for the wt FabI and (F203L)FabI interaction with NADH were found to be 4.2 ± 0.6 and 1.8 ± 0.9 μM, respectively, with stoichiometries of 0.91 ± 0.01 per wt FabI monomer and 0.86 ± 0.06 per (F203L)FabI monomer. Thus, there are no significant differences between the binding constants and stoichiometries for NADH binding to the wt and mutant protein in comparison to those in the published literature. This is noteworthy because, as described next, binding stoichiometries for inhibitors deviated from those found for cofactor binding.

Energetics of wt FabI and (F203L)FabI Binding to 2-(2-Hydroxyphenoxy)phenols. It has previously been shown that the formation of a ternary FabI−NAD^+−inhibitor complex is necessary to achieve inhibition (*10*, *11*, *13*, *31*), suggesting that inhibitors have poor or no affinity for the apoenzyme. Therefore, all inhibitor-binding experiments were conducted in the presence of excess (0.5 mM) NAD^+. The thermodynamic parameters for wt FabI−NAD^+ and (F203L)FabI−NAD^+ binding of inhibitors were obtained by ITC in the temperature range of 15−30 °C. An example of ITC data for binding of compound PD048890 [2-(2-hydroxyphenoxy)-phenol, Figure 1A] to FabI−NAD^+ is shown in Figure 6. Similar experiments were carried out for 4-alkyl-substituted 2-(2-hydroxyphenoxy)phenols with alkyl substituents varying from methyl to *n*-propyl (parts B−D of Figure 1). The results of all wt FabI and (F203L)FabI ITC experiments are presented in Table 2 and Table 3, respectively.

As seen in Tables 2 and 3, inhibitor affinity increases with aliphatic side-chain length, as expected from the enzyme inhibition data shown in Figure 5. A notable feature of the ITC experiments is the absence of a measurable heat effect with (F203L)FabI titration by 2-(2-hydroxyphenoxy)phenol ($R = H$, PD048890). This could be due to the fortuitous coincidence of a zero binding enthalpy at the ITC temperature of measurement, but this is unlikely, because the inhibitor has no measurable effect on the enzymatic activity of the enzyme (Figure 5B). DSC of (F203L)FabI alone and in the presence of excess 2-(2-hydroxyphenoxy)phenol also did not show any difference in contrast to complexes with other inhibitors (for example, with PD205405, Figure 4C). Col-

Table 2: Thermodynamic Parameters of wt FabI Interaction with Inhibitors in the Presence of 0.5 mM NAD^+ in 10 mM Na-phosphate Buffer at pH 7.5, 2% DMSO, 1 mM EDTA, and 1% Glycerol

inhibitor	T (°C)	ΔG (kJ/mol)	K_d (nM)	ΔH (kJ/mol)	ΔS (J K^{-1} mol^{-1})	n	ΔC_p (kJ K^{-1} mol^{-1})
PD048890	15	−41.7	28 (1.5)	−42.5 (0.8)	−2.6	0.54 (0.01)	
PD048890	20	−40.8	54 (15)	−56.9 (0.8)	−54.4	0.63 (0.01)	
PD048890	25	−39.0	100 (40)	−84.9 (2.0)	−153.6	0.55 (0.02)	
PD048890	30	−40.5	110 (25)	−95.0 (1.6)	−179.9	0.61 (0.01)	−3.69 (0.67)
PD200828	20	−46.6	5.0 (2.0)	−72.8 (0.8)	−89.1	0.60 (0.003)	
PD200828	25	−45.8	10.0 (5.0)	−81.2 (1.2)	−118.8	0.65 (0.01)	
PD200828	30	−46.5	12.0 (3.0)	−106.3 (1.6)	−197.1	0.63 (0.01)	−3.35 (0.96)
PD202165	25	−50.2	1.6 (1.2)	−73.2 (1.2)	−77.4	0.70 (0.005)	
PD202165	27.5	−49.5	2.5 (1.2)	−88.3 (1.2)	−128.9	0.69 (0.004)	
PD202165	30	−48.2	5.0 (2.0)	−98.3 (0.8)	−165.3	0.73 (0.003)	−5.03 (0.57)
PD205405	25	−49.0	1.4 (0.7)	−68.7 (0.8)	−66.4	0.73 (0.003)	
PD205405	27.5	−46.0	9.6 (6.0)	−81.6 (2.0)	−118.4	0.62 (0.006)	
PD205405	30	−48.8	4.0 (1.0)	−93.3 (0.8)	−146.9	0.69 (0.003)	−5.36 (0.38)

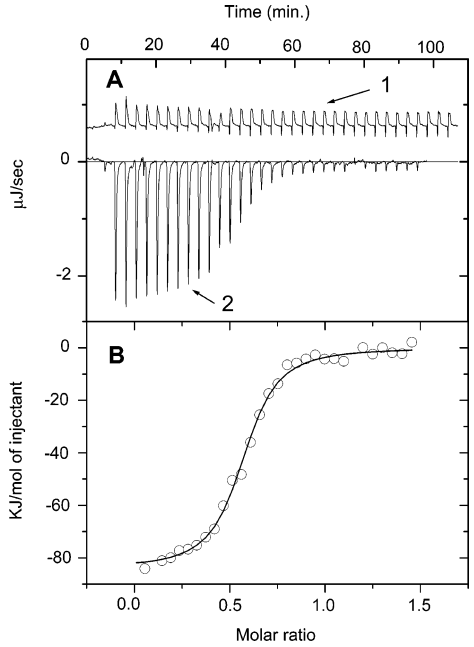

FIGURE 6: Representative data from an ITC experiment. The cell (1.34 mL) contained 13.0 μM wt FabI in 10 mM Na-phosphate buffer at pH 7.5, 2% (v/v) DMSO, 1 mM EDTA, 1% glycerol, and 0.5 mM NAD^+ at 25 °C. (A) raw data of injections of inhibitor, PD048890, into buffer, inhibitor dilution effect (1); raw data of protein titration by PD048890 with integration baseline (2). (B) Data after peak integration, subtraction of inhibitor dilution effect, and concentration normalization. The solid line is the fit to a single binding site model. Results of the curve fitting are shown in Tables 2 and 3.

lectively, such evidence supports the conclusion that (F203L)FabI−NAD^+ does not interact with 2-(2-hydroxyphenoxy)phenol.

Molecular Basis for Enthalpy, Entropy, and Heat Capacity Changes. The binding of all inhibitors to wt or mutant FabI−NAD^+ is characterized by a favorable enthalpy change and by an unfavorable entropy change (Tables 2 and 3). However, the systematic increase in affinity with increasing aliphatic chain length is entropically driven because the binding enthalpy becomes less favorable and the entropy becomes more favorable. These trends are graphically represented for a single measurement temperature, 25 °C, in Figure 7, in which each thermodynamic binding parameter is plotted as a function of the aliphatic side-chain ASA of the inhibitor.

Increasing the compound aliphatic side-chain length increases the hydrophobicity of the inhibitors, and thus, changes in solvation upon binding are probably responsible for the increase in entropy with increasing aliphatic chain length, as the following analysis suggests. The total binding entropy (ΔS_{total}) can be partitioned into contributions from the solvation entropy change (ΔS_{solv}), the entropy change because of the loss of conformational flexibility, which are included in (ΔS_{other}), and a translational or cratic term (ΔS_{trans}) as follows (*28*): $\Delta S_{total} = \Delta S_{solv} + \Delta S_{trans} + \Delta S_{other}$, where $\Delta S_{trans} \cong -42$ J/mol K, is a lower limit for the loss of translational entropy (*32*). The solvation entropy change at a given temperature T can be estimated from $\Delta S_{solv} = \Delta C_p \ln(T/385)$ (*28*). Assuming ΔC_p is temperature independent, linear regression analysis of enthalpy versus temperature data yields the ΔC_p values (reported in Tables 2 and 3). These are plotted in Figure 7B. The negative signs and magnitudes of the ΔC_p indicate that desolvation contributes significantly to the binding of these inhibitors, consistent with the calculated values for ΔS_{solv}, shown in Figure 7C. Also shown in Figure 7C is ΔS_{other}, which becomes more negative with the increasing aliphatic chain length, somewhat offsetting the positive influence of ΔS_{solv}.

ΔC_p is large and negative for both proteins, although it is significantly smaller for the mutant. There is a difference [$\Delta(\Delta C_p)$] of approximately -1.97 ± 0.34 kJ K^{-1} mol^{-1} between the wt and mutant binding ΔC_p for any given inhibitor; in fact, this difference is fairly constant (Figure 7). The difference in ΔC_p (as well as in ΔS_{solv} and ΔS_{other}) may be explained, in part, by the preordering of the mutant substrate-binding loop. The X-ray crystal structure of the binary complex of (F203L)FabI with NAD^+ has been determined (unpublished data) and clearly shows that the flexible substrate-binding loop is completely folded, unlike that for the binary complex of the wt (see Figure 8). Therefore, folding of the flexible substrate-binding loop occurs only in the wt protein upon ternary complex formation, and this conformational change will contribute to the differences in observed thermodynamic parameters.

However, a further question is, is the difference in the conformational change of the substrate-binding loop sufficient to explain the experimentally derived $\Delta(\Delta C_p)$ between the wt and mutant or are there other differences between the structures upon inhibitor binding? Calculated ΔC_p values can be obtained for the binding of each protein to the inhibitor from estimates of the change in ASA derived from crystal structures of the respective binary and ternary complexes (*28*, *29*). A comparison of the respective calcu-

Table 3: Thermodynamic Parameters of (F203L)FabI Mutant Interaction with Inhibitors in the Presence of 0.5 mM NAD^+ in 10 mM Na-phosphate Buffer at pH 7.5, 2% DMSO, 1 mM EDTA, and 1% Glycerol

inhibitor	T (°C)	ΔG (kJ/mol)	K_d (nM)	ΔH (kJ/mol)	ΔS (J K^{-1} mol^{-1})	n	ΔC_p (kJ K^{-1} mol^{-1})
PD200828	15	−36.4	2.4 (1.1)	−59.4 (5.0)	−79.9	0.53 (0.03)	
PD200828	20	−34.3	0.77 (0.15)	−62.3 (5.0)	−96.7	0.48 (0.03)	
PD200828	25	−35.1	0.74 (0.07)	−73.2 (2.5)	−128.0	0.45 (0.01)	−1.38 (0.46)
PD202165	15	−35.2	0.42 (0.09)	−36.4 (1.2)	−4.2	0.47 (0.01)	
PD202165	20	−36.6	0.35 (0.05)	−53.1 (1.2)	−56.5	0.52 (0.01)	
PD202165	25	−38.9	0.24 (0.06)	−59.1 (2.5)	−68.0	0.49 (0.01)	−2.51 (0.42)
PD205405	15	−37.7	0.14 (0.04)	−28.4 (0.8)	+32.2	0.58 (0.001)	
PD205405	20	−38.6	0.13 (0.02)	−48.5 (3.3)	−33.9	0.61 (0.01)	
PD205405	25	−35.4	0.65 (0.15)	−66.1 (3.3)	−102.9	0.54 (0.02)	−3.81 (0.13)

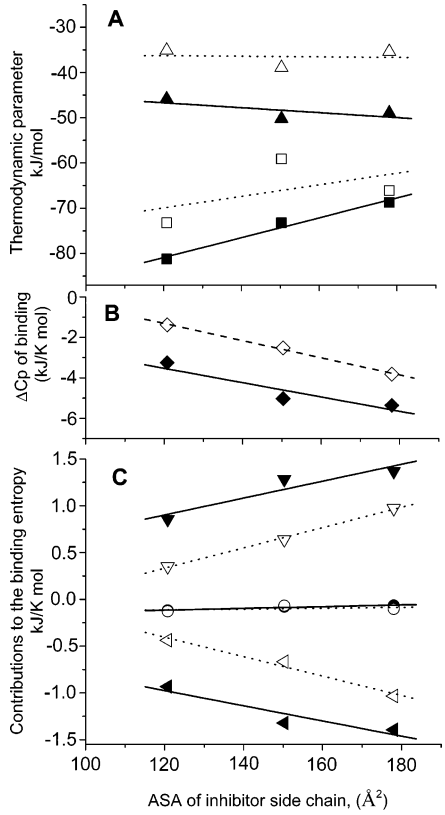

FIGURE 7: Relationship between thermodynamic parameters of FabI−NAD^+ binding to inhibitors and the ASA of the side chain at 25 °C. Solid symbols and lines, wt FabI; open symbols and dotted lines, (F203L)FabI. Values are taken from Tables 2 and 3. (A) ΔG (▲, △); ΔH (■, □). (B) ΔC_p, (◆, ◇). (C) ΔS_{total} (●, ○); ΔS_{solv} (▼, ▽); ΔS_{other} (tilted ▲, tilted △). ASA of side chains were approximated by the published ASA for methane = 120.8 Å² for PD020828, ethane = 150.3 Å² for PD0202165, and propane = 178.0 Å² for PD0205405 (*34*).

lated and experimental ΔC_p [and $\Delta(\Delta C_p)$] for each protein would help answer this question. Because all of the crystal structures are not available for this calculation, an alternative approach has been used that makes use of wt binary and ternary crystal structures that are available. From these, estimated ΔC_p values were obtained from measured changes in polar and apolar ASA (*28*, *29*; see the Experimental Procedures for details). Two ΔC_p were calculated. The first estimates just the contribution from loop ordering upon ligand binding, and this value is −0.75 kJ K^{-1} mol^{-1}. A second calculation estimates the additional contributions made by any small or distributed changes in ASA in the rest of the protein, in addition to loop ordering. For this calculation, FabI crystal structures of a binary (inhibitor-free) complex and a ternary complex with an alternative inhibitor were used

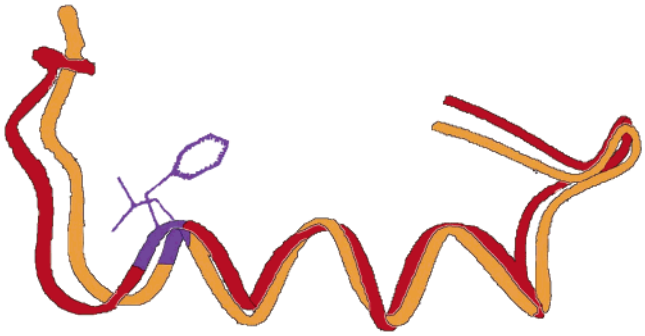

FIGURE 8: Superposition of the backbone of amino acid residues 196−219 in wt FabI (red) in complex with NAD^+ and thienodiazaborine (PDB 1DFH, *10*) and that of (F203L)FabI (orange) with NAD^+ alone. Phe203 of wt FabI and Leu203 of (F203L)FabI are shown in violet, using the Insight II software (version 97.1, Molecular Simulations, Inc).

(*10*). In this case, the value of $\Delta(\Delta C_p)$ is −1.80 kJ K^{-1} mol^{-1}. This latter value reflects the change in loop ordering plus the change in the remaining structure upon inhibitor binding. Because this value is very similar to the experimental value of $\Delta(\Delta C_p)$, it suggests that in the presence of an ordered substrate-binding loop there are additional, apparently more distributed changes in other regions of the protein, which are not obvious by mere inspection of the crystal structures. For the binary complex of (F203L)FabI, all of these changes have occurred before inhibitor binding, while for the binary complex of wt FabI, these changes occur along with inhibitor binding and are, therefore, detected in the ITC experiment.

Enzyme Inhibitor Binding Stoichiometry and Tetramer Structural Cooperativity. Both the wt and mutant apoenzymes bind the cofactor NADH with a stoichiometry of approximately one per monomer (four per tetramer). In contrast, the stoichiometry for binding of inhibitors to the binary complexes (wt FabI−NAD^+ and (F203L)FabI−NAD^+) is closer to 0.5 (see Tables 2 and 3). Because the structural unit is a tetramer containing four binding sites, this stoichiometry is equivalent to the binding of only two inhibitors per tetramer. This result suggests that there is negative cooperativity for binding after two of the binding sites are filled, resulting in two conformationally distinct dimeric pairs upon half-site occupancy. Unfortunately, it was not technically possible to extend the calorimetric titration up to concentrations of the inhibitor that might have allowed the observation of binding to the second set of binding sites, although a hint of this is observed for the binding of some inhibitors to wt FabI. That is, on closer inspection of the binding ITC stoichiometries given in Tables 2, a trend is noticed for the stoichiometry to increase from ~0.5 to ~0.7 with an increasing aliphatic chain length. As noted above,

inhibitor binding is associated with the ordering of the flexible loop residues 196−206 for the wt, but this does not seem to be the structural basis for negative cooperativity upon half-site occupancy because this loop is preordered in the mutant, which also exhibits negative cooperativity. Furthermore, there does not seem to be a significant change in the homotetramer organization upon ternary complex formation [excluding the loop movement, which is not near the packing interface of the tetramer (*33*)] based on published X-ray crystal structures, even though the comparison between calculated and experimental $\Delta(\Delta C_p)$ just discussed suggests some change in the structure upon binding that is not obvious from the complex crystal structures. Interestingly, only two molecules of 2-(2-hydroxyphenoxy)phenol per wt FabI tetramer are observed in the crystal structure of their complex, which is consistent with the finding obtained by ITC. Further support for the change in binding cooperativity and stoichiometry comes from the observed change in the unfolding cooperativity determined by DSC. The $\Delta H_{vH}/\Delta H_{cal}$ ratio for the thermal unfolding of both ternary complexes (Figure 4C) indicates that the cooperative unit is only a dimer, whereas for the main transition of both the wt and mutant apoenzymes, it is the tetramer.

However, there are other possible explanations for the reduced stoichiometry. An impure protein or partially unfolded protein would cause the concentration of the active protein to be lower, but this can be ruled out on the basis of the CD and DSC results, as well as the stoichiometry of NADH binding, all of which are consistent with a completely and correctly folded protein and which require input of the protein concentration to achieve the results shown. Alternatively, underestimation of inhibitor concentration would also result in reduced stoichiometries. While this possibility cannot be unequivocally ruled out, it is unlikely to be the cause of the lower than expected stoichiometries, simply based on the trends observed in the inhibitor series and the corroborating X-ray and DSC data.

Comparison of wt FabI and (F203L)FabI Binding Energetics: Model for Resistance. Previously discussed was the apparent linear relationship between the ASA of the inhibitor aliphatic side chain and each thermodynamic parameter, as shown in Figure 7. The same trends for the wt and mutant suggest that changes in the inhibitor affinity are dominated by the hydrophobicity of the side chain for both proteins. However, the lines do not superimpose, suggesting that some structural difference in the binding site causes the observed absolute difference in the binding affinities resulting in the resistance of (F203L)FabI. While preordering of the substrate-binding loop in the mutant may account for the absolute differences, inspection of many published ternary complexes provides an additional possible explanation. Because structures of complexes with 2-(2-hydroxyphenyl)phenol and its derivatives with either wt FabI or (F203L)FabI are unknown, an alternative published ternary FabI−NAD^+−inhibitor complex (PDB 1DFH, *10*) was used to superimpose the substrate-binding loop onto the structure of the (F203L)-FabI loop in its binary complex with NAD^+. The resulting overlay shows that the loop structures are essentially the same (Figure 8) and shows the location and volume needed for inhibitor binding to the mutant. It is apparent from the model that the introduction of Leu at position 203 may require the inhibitor aliphatic side chain to occupy a different region of the binding pocket. Preordering of the flexible substrate-binding loop prior to inhibitor binding in the case of the mutant may also eliminate the ability of the substrate-binding loop to adopt alternative conformations that would be energetically more favorable. This possibility can be inferred from the multiple conformations observed for this loop when diazaborine inhibitors bind (*8*). It is interesting that relative structural rigidity has also been proposed as a basis for drug resistance in HIV protease (*16*−*19*). Like the present studies, Freire and colleagues utilized details from a calorimetric evaluation of thermodynamic binding parameters to reach their conclusions, but in those studies, conformational rigidity of the inhibitor and not the protein was the cause for the decreased inhibitor affinity.

Conclusions. The key observations of this study provide both structural and energetic insights into the mechanism of inhibitor binding to wt FabI. A plausible mechanism for (F203L)FabI drug resistance is also offered that is likely derived from a combination of two factors, an altered inhibitor-binding mode and a relatively more rigid binding site for the mutant. Also new to this paper is the observation of an apparent negative cooperativity for inhibitor binding to wt FabI.

ACKNOWLEDGMENT

We are grateful to Naeja Pharmaceuticals Laboratory for the syntheses of some compounds and Steve Vander Roest, Antibacterial Pharmacology, Pfizer Global Research and Development, Ann Arbor, MI, for the initial cloning of wt FabI.

REFERENCES

1. Heath, R. J., and Rock, C. O. (1995) Enoyl-acyl carrier protein reductase (FabL) plays a determinant role in completing cycles of fatty acid elongation in *Escherichia coli*, *J. Biol. Chem. 270*, 26538−26542.
2. Heath, R. J., Li, J., Roland, G. E., and Rock, C. O. (2000) Inhibition of the *Staphylococcus aureus* NADPH-dependent enoyl-acyl carrier protein reductase by triclosan and hexachlorophene, *J. Biol. Chem. 275*, 4654−4659.
3. Heath, R. J., Rubin, J. R., Holland, D. R., Zhang, E., Snow, M. E., and Rock, C. O. (1999) Mechanism of triclosan inhibition of bacterial fatty acid synthesis, *J. Biol. Chem. 274*, 11110−11114.
4. Stewart, M. J., Parikh, S., Xiao, G., Tonge, P. J., and Kisker C. (1999) Structural basis and mechanism of enoyl reductase inhibition by triclosan, *J. Mol. Biol. 290*, 859−865.
5. Levy, C. W., Roujeinikova, A., Sedelnikova, S., Baker, P. J., Stuitje, A. R., Slabas, A. R., Rice, D. W., and Rafferty, J. B. (1999) Molecular basis of triclosan activity, *Nature 398*, 383−384.
6. Roujeinikova, A., Levy, C. W., Rowsell, S., Sedelnikova, S., Baker, P. J., Minshull, C. A., Mistry., A., Colls, J. G., Camble, R., Stuitje, A. R., Slabas, A. R., Rafferty, J. B., Pauptit, R. A., Viner, R., and Rice, D. W. (1999) Crystallographic analysis of triclosan bound to enoyl reductase, *J. Mol. Biol. 294*, 527−535.
7. Baldock, C., Rafferty, J. B., Stuitje, A. R., Slabas, A. R., and Rice, D. W. (1998) The X-ray structure of *Escherichia coli* enoyl reductase with bound NAD^+ at 2.1 Å resolution, *J. Mol. Biol. 284*, 1529−1546.
8. Levy, C. W., Baldock, C., Wallace, A. J., Sedelnikova, S., Viner, R. C., Clough, J. M., Stuitje, A. R., Slabas, A. R., Rice, D. W., and Rafferty J. B. (2001) A study of the structure−activity relationship for diazaborine inhibition of *Escherichia coli* anoyl-ACP reductase, *J. Mol. Biol. 309*, 171−180.
9. Dessen, A., Quemard, A., Blanchard, J. S., Jacobs, W. R., and Sacchettini, J. C. (1995) Crystal structure and function of the isoniazid target of *Mycobacterium tuberculosis*, *Science 267*, 1638−1641.
10. Baldock, C., Rafferty, J. B., Sedelnikova, S. E., Baker, P. J., Stuitje, A. R., Slabas, A. R., Hawkes, T. R., and Rice, D. W. (1996) A

mechanism of drug action revealed by structural studies of enoyl reductase, *Science 274*, 2107−2110.
11. Heath, R. J., Yu, Y. T., Shapiro, M. A., Olson, E., and Rock, C. O. (1998) Broad spectrum antibacterial biocides target the FabI component of fatty acid synthesis, *J. Biol. Chem. 273*, 30316−30320.
12. McMurry, L. M., Oethinger, M., and Levy, S. B. (1998) Triclosan targets lipid synthesis, *Nature 394*, 531−532.
13. Sivaraman, S., Zwahlen, J., Bell, A. F., Hedstrom, L., and Tonge, P. J. (2003) Structure−activity studies of the inhibition of FabI, the enoyl reductase from *Escherichia coli*, by triclosan: Kinetic analysis of mutant FabIs, *Biochemistry 42*, 4406−4413.
14. Parker, M. H., Lunney, E. A., Ortwine, D. F., Pavlovsky, A. G., Humblet, C., and Brouillette, C. G. (1999) Analysis of the binding of hydroxamic acid and carboxylic acid inhibitors to the stromelysin-1 (matrix metalloproteinase-3) catalytic domain by isothermal titration calorimetry, *Biochemistry 38*, 13592−13601.
15. Leavitt, S., and Freire, E. (2001) Direct measurement of protein binding energetics by isothermal titration calorimetry, *Curr. Opin. Struct. Biol. 11*, 560−566.
16. Luque, I., Todd, M. J., Gomez, J., Semo, N., and Freire, E. (1998) Molecular basis of resistance to HIV-1 protease inhibition: A plausible hypothesis, *Biochemistry 37*, 5791−5797.
17. Velázquez-Campoy, A., Todd, J. J., and Freire, E. (2000) HIV-1 protease inhibitors: Enthalpic versus entropic optimization of the binding affinity, *Biochemistry 39*, 2201−2207.
18. Todd, M. J., Luque, I., Veláquez-Campoy, A., and Freire, E. (2000) Thermodynamic basis of resistance to HIV-1 protease inhibition: Calorimetric analysis of the V82F/I84V active site resistant mutant, *Biochemistry 39*, 11876−11883.
19. Muzammil, S., Ross, P., and Freire, E. (2003) A major role for a set of non-active site mutations in the development of HIV-1 protease drug resistance, *Biochemistry 42*, 631−638.
20. Gill, S. C., and von Hipple, P. H. (1989) Calculation of protein extinction coefficients from amino acid sequence data, *Anal. Biochem. 182*, 319−326.
21. Peterson, G. L. (1977) A simplification of the protein assay method of Lowry et al. which is more generally applicable, *Anal. Biochem. 83*, 346−356.
22. Kime, D. E., and Norymberski, J. K. (1977) Synthesis of fully aromatic cyclic polyethers, *J. Chem. Soc., Perkin Trans. 1*, 1048−1052.
23. Bergler, H., Fuchsbichler, S., Hogenauer, G., and Turnowsky, F. (1996) The enoyl-[acyl-carrier-protein] reductase (FabI) of *Escherichia coli*, which catalyzes a key regulatory step in fatty acid biosynthesis, accepts NADH and NADPH as cofactors and is inhibited by palmitoyl-CoA, *Eur. J. Biochem. 242*, 689−694.
24. Ward, W. H. J., Holdgate, G. A., Rowsell, S., McLean, E. G., Pauptit, R. A., Clayton, E., Nichols, W. W., Colls, J. G., Minshull, C. A., Jude, D. A., Mistry, A., Timms, D., Camble, R., Hales, N. J., Britton, C. J., and Taylor, I. W. F. (1999) Kinetic and structural characteristics of the inhibition of enoyl (acyl carrier protein) reductase by triclosan, *Biochemistry 38*, 12514−12525.
25. Wiseman, T., Williston, S., Brandts, J. F., and Lin, L. N. (1989) Rapid measurement of binding constants and heats of binding using a new titration calorimeter, *Anal. Biochem. 179*, 131−137.
26. Indyk, L., and Fisher, H. F. (1998) Theoretical aspects of isothermal titration calorimetry, *Methods Enzymol. 295*, 350−364.
27. Connolly, M. L. (1993) The molecular surface package, *J. Mol. Graphics 11*, 139−141.
28. Baker, B. M., and Murphy, K. P. (1998) Prediction of binding energetics from structure using empirical parameterization, *Methods Enzymol. 295*, 294−315.
29. Gomez, J., and Freire, E. (1995) Thermodynamic mapping of the inhibitor site of the aspartic protease endothiapepsin, *J. Mol. Biol. 252*, 337−350.
30. Privalov, P. L., and Potekhin, S. A. (1986) Scanning microcalorimetry in studying temperature-induced changes in proteins, *Methods Enzymol. 131*, 4−51.
31. Quemard, A., Sacchettini, J. C., Dessen, A., Vilcheze, C., Bittman, R., Jacobs, W. R., and Blanchard, J. S. (1995) Enzymatic characterization of the target for isoniazid in mycobacterium tuberculosis, *Biochemistry 34*, 8235−8241.
32. Amzel, L. M. (1997) Loss of translational entropy on binding, folding, and catalysis, *Proteins 28*, 144−149.
33. Rozwarski, D. A., Vilcheze, C., Sugantino, M., Bittman, R., Sacchettini, J. C. (1999) Crystal structure of the mycobacterium tuberculosis enoyl-ACP reductase, InhA, in complex with NAD^+ and a C16 fatty acyl substrate, *J. Biol. Chem. 274*, 15582−15589.
34. Madan, B., and Sharp, K. (1997) Molecular origin of hydration heat capacity changes of hydrophobic solutes: Perturbation of water structure around alkanes, *J. Phys. Chem. B 101*, 11237−11242.

BI0492509